Sensitivity of crossflow surfacetransitionroughnessto free-stream conditions and

Rizzo, Paolo; Serpieri, Jacopo; Kotsonis, Marios

DOI
10.2514/6.2019-1133

Publication date
2019

Document Version
Final published version

Published in
AIAA Scitech 2019 Forum

AIAA SciTech Forum
7-11 January 2019, San Diego, California
AIAA Scitech 2019 Forum

10.2514/6.2019-1133

Sensitivity of Crossflow Transition to Free-Stream Conditions and Surface Roughness

Paolo Rizzo*, **Jacopo Serpieri**†, **Marios Kotsonis**‡

Section of Aerodynamics, Faculty of Aerospace Engineering, Delft University of Technology, Kluyverweg 1, 2629HS Delft, The Netherlands

The present work is an experimental investigation of stationary crossflow (CF) instability-induced transition of the boundary layer over a 45°swept wing, under varying free-stream turbulence, surface roughness, angle of attack and Reynolds number. Key topological features of the transition front, such as the mean transition location and the jaggedness of the front, are retrieved via IR thermography. Linear Stability Theory (LST) is used to extract the N-factor of the most amplified stationary crossflow mode at the transition location, identified experimentally. Results show clear causality between free-stream turbulence, surface roughness, Reynolds number, angle of attack and transition. Large losses of laminarity and a consistent decrease in the transition N-factor are observed with rising turbulence and roughness. Remarkably, N-factor sensitivity to free-stream turbulence is found to vary significantly and non-linearly with angle of attack for the modest levels of turbulence explored in this campaign, whereas the N-factors scale linearly with the log of the surface roughness level, which is consistent with a receptivity mechanism, which is independent of the angle of attack.

Nomenclature

α = airfoil angle of attack
α_i = imaginary component of the streamwise wavenumber
α_r = real component of the streamwise wavenumber
β_i = imaginary component of the spanwise wavenumber
β_r = real component of the spanwise wavenumber
λ_z = z-wavelength
ω = angular frequency
σ_{tr} = standard deviation of points on transition front about mean transition line
c = chord length in the swept system
c_X = chord length in the unswept system
j = jaggedness of the transition front
N^{SCF} = N-factor of the critical stationary crossflow instability mode at transition
q = perturbation eigenfunction
R_q = root-mean-square (RMS) surface roughness
Re = Reynolds number
Tu = free-stream turbulence
U_∞ = free-stream velocity in wind tunnel coordinates
X = chordwise direction in the unswept system
x = chordwise direction in the swept system
X^p_{tr} = mean transition location in pixel
x_t = local chordwise direction
X_{tr} = mean transition location in the unswept system
Y = wall-normal direction in the unswept system
y = wall-normal direction in the swept system
y_t = local wall-normal direction
Z = spanwise direction in the unswept system
z = spanwise direction in the swept system
z_t = local spanwise direction

*M.Sc. Student, Faculty of Aerospace Engineering
†Research Fellow, Faculty of Aerospace Engineering
‡Assistant Professor, Faculty of Aerospace Engineering

I. Introduction

SWEPT wing boundary layers are often subject to laminar-turbulent transition due to the growth and laminar breakdown of crossflow (CF) instability mechanisms. These instabilities arise due to the inherent three-dimensionality of swept wing boundary layer flows. The relative lack of momentum within the boundary layer causes air particles to experience a local force imbalance, compared to the inviscid flow configuration, in a direction orthogonal to the streamlines and parallel to the wing surface, inducing motion in the direction opposite to the pressure gradient. Physically, this inflectional boundary layer profile is inherently unstable and entails the development of a series of streamwise-oriented co-rotating vortical disturbances that redistribute momentum within the boundary layer. These instability modes can be of a stationary or traveling nature, depending on boundary layer receptivity to free stream conditions and surface roughness, and have been found to have a distinctive effect on the topology of the transition front. The spanwise velocity modulation caused by the crossflow vortices can be observed via visualization methods such as infrared thermography, napthalene sublimation or fluorescent oil coatings; stationary modes appear as a series of surface streaks aligned within a few degrees to the mean flow direction.

Given the low levels of free stream turbulence in free

flight, stationary crossflow disturbances are a common catalyst for transition under typical flight conditions, and have been shown to sharply promote the transition front upstream, adversely affecting aerodynamic performance. Among the most striking properties of crossflow transition mechanisms is their intrinsic and intricate dependence on initial conditions and free-stream properties, which has been investigated extensively but deserves further attention due to its industrial relevance. Uncovering knowledge on this complex dependence will make way for novel opportunities to (actively or passively) control the growth of crossflow disturbances to delay transition.

This paper is devoted to shedding further light on the intricate relationship between free-stream turbulence, surface roughness and the growth and breakdown of crossflow instability modes which lead to laminar-turbulent transition, under different pressure distributions and Reynolds number flow conditions.

II. Literature Overview

Leading experimental campaigns on the behavior of three-dimensional boundary layers were conducted in Germany (Deutsches Zentrum für Luft- und Raumfahrt (DLR) Göttingen) by Bippes and coworkers [8] [2] and in the United States, by William Saric and his group (Arizona State University first and later at Texas A&M University) [15]. Paired with more recent efforts making use of direct numerical simulation (DNS)[21] and innovative optical flow diagnostics [18], these studies have helped reveal important information on the development of crossflow disturbances and their sensitivity to free-stream parameters, shedding light on several aspects of the complex transition patterns they induce. In particular, this section will focus on summarizing the most relevant results to-date regarding the effect of angle of attack, Reynolds number, free stream turbulence and distributed surface roughness on the growth and breakdown of crossflow modes.

Increasing Reynolds number has been found to move transition upstream, and increase the rate of CF disturbance growth [14]; furthermore, higher Reynolds numbers appear to force higher frequency crossflow modes [17] [2] [9].

Extensive investigations on the role of modest levels of free-stream turbulence intensity (ranging from 0.02% to 0.19% of freestream velocity) on crossflow disturbances were conducted by Downs and White [9]. Turbulence levels were varied by means of passive turbulence grids positioned upstream of the model. Results showed that increasing the turbulence level does not appear to affect the initial disturbance amplitude significantly; in the presence of spanwise roughness arrays near the leading edge, baseline amplitudes at different turbulence levels only differed by values smaller than the estimated experimental error. The effect on disturbance development, instead, was found to be much larger than that on receptivity.

When analyzing the effect on amplitude growth, Downs and White found that with rising turbulence levels the stationary mode was reduced in amplitude. At Tu = 0.19% significant attenuation of the latter was observed after 30% of the chord, although the same mode underwent amplification at 30% of the chord for turbulence intensities lower than 0.05%. Unsteady (travelling) disturbances, instead, were found to undergo larger growth rates in the higher turbulence environments. This stands to confirm that, contrary to travelling modes, stationary modes amplify more vigorously in low turbulence environments.

Turbulence intensity also proved to have important effects on the observed transition pattern. Generally, with rising turbulence levels, the transition front width was found to decrease [9]. This is because travelling disturbance amplification is promoted at the expense of stationary mode growth. Unsteady modes tend to distribute the spanwise velocity modulation of the boundary layer, which has a 'smoothening' effect on the transition front and gives it a less jagged appearance. This is particularly evident in the natural roughness case when no stationary modes are purposely stimulated, and the most severe drop in transition front width is observed. In low-turbulence environments, transition is dominated by the stationary crossflow instability, which is very sensitive to roughness. The experiments of Radetzsky et al.[13] and Crouch and Ng[5] show promising applications of the variable N-factor approach, linking crossflow transition to surface roughness for transition prediction under low free-stream turbulence. Similar approaches were also applied in the presence of surface steps[3][20]. Under moderate to high turbulence intensities, however, the travelling crossflow instability modes dominate and the variable N-factor fails to accurately capture the causality between roughness amplitude and transition, suggesting that stationary and travelling modes can have a coupled effect on transition that is highly non-linear. The present work focuses on uncoupling the effect of turbulence and roughness and explores a domain in which it is sensible to ignore the underlying non-linear physics of transition and apply linear theory at least for the initial stages of instability growth. It is of course important to note that eventual laminar breakdown is summoned by the non-linear saturation of primary crossflow modes and subsequent development of secondary instabilities, thus rendering LST inapplicable for the later stages of transition [10].

Few experiments have been conducted to date concerning the coupled effect of angle of attack with free-stream turbulence or surface roughness on crossflow transition. This study, therefore, is also concerned with deploying linear theory to infer causality between varying angle of attack, free-stream turbulence, distributed surface roughness and crossflow transition.

III. Experimental Setup

A. Wind Tunnel Facility and Model

For this experimental campaign, a 45°swept wing model with no twist or taper was chosen. Unlike TS instabilities, crossflow disturbances amplify in favorable pressure gradients [2]. In order to exploit this property, a highly laminar wing section, namely the 66018 M3J (shown in Figure 1), was designed by modifying the NACA 66018 airfoil used in the experiments of Saric et al. [15]. The negative pressure gradient region was prolonged to approximately 70 % of the chord at neutral incidence, rendering the model sub-critical to TS disturbances. Furthermore, the airfoil was adapted to feature a small leading edge radius of approximately 1 % in order to prevent attachment line instability and no concave shape to avoid the formation of Görtler vortices [2] [17].

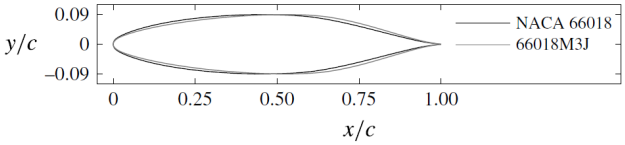

Figure 1. 66018 M3J airfoil used in the present campaign compared to the NACA 66018. Figure taken from [18].

The model features a chord of approximately 1.3m in the freestream direction and was installed in the Low Turbulence Tunnel (LTT) facility at Delft University of Technology (a closed loop, low turbulence subsonic wind tunnel with a 125cm x 180cm x 260cm test section, height, width, and length respectively), spanning the entire test section in height and length [17].

Given the complexity of swept-wing boundary layer flow, it is imperative to provide an overview of the unswept and swept coordinate systems used for analysis, a visual representation of which is given in Figure 2. The unswept coordinate system, denoted by *XYZ* and with velocity components *UVW*, is aligned with the wing chord plane, which is oriented at an angle of incidence α to the reference system of the wind tunnel. Velocity components in the wind tunnel system are denoted with the subscript ∞; for instance, the free-stream velocity U_∞ used to normalize the free-stream turbulence is defined in the wind tunnel coordinate system. The swept coordinate system *xyz* with velocity components *uvw*, instead, has z aligned with the leading edge of the model and x perpendicular to it; it is a clockwise rotation of *XYZ* by the leading edge sweep (Λ = 45°) about the Y axis. The transition locations X_{tr}/c_X in Figure 7 are given in the unswept system. However, the LST problem discussed in section IV is formulated and solved in the swept coordinate system with swept chord stations *x/c*. The other coordinate system shown in Figure 2 is the local tangential system ($x_t y_t z_t$), which follows the curvature of the airfoil along the X (unswept) direction such that x_t is always tangent to the surface, y_t is the wall-normal direction and z_t coincides with the Z axis.

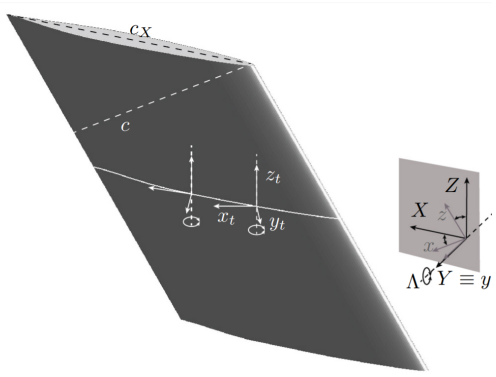

Figure 2. Schematic of the wind tunnel model with airfoil 66018 MRJ showing the unswept (XYZ), swept (xyz) and local tangential ($x_t y_t z_t$) coordinate systems. c_X represents the chord along the unswept X axis, whereas c is the chord along the swept x axis. Figure taken from [18].

Thermographic scans of the pressure side of the model were conducted under different flow conditions, namely at varying angle of attack, Reynolds number, free-stream turbulence and surface roughness. Relying on IR thermography as primary means of flow visualization allowed for a multitude of different flow cases to be analyzed efficiently and with sufficient accuracy to quantify characteristics of the associated transition pattern, based on the inherent differences of covective heat flux assosciated with laminar and turbuent flows [19] [16] [22]. In order to sustain sufficient contrast for the IR imager, the wing model was irradiated with six 1W halogen lamps through glass windows in the test section. An Optris PI640 IR camera with a thermal sensitivity of 75 mK, operating in the 7.5-13 µm spectral band, was used to obtain surface temperature distributions. The measurements were cast to the *XZ* plane by means of a spatial mapping (i.e. dewarping) obtained from calibration images at several angles of attack. The IR camera registered 100 images at a rate of 5Hz for every case once the temperature distribution had reached an equilibrium; these were averaged in order to enhance the signal-to-noise ratio. It must be noted that the measured distributions were not further corrected for emissivity or reflectivity, given that they were used to extract the transition location and standardized width (jaggedness) of the

transition front.

B. Free-Stream Turbulence variations

Table 1 shows an overview of all flow cases tested in this study. The LTT facility is furbished with 9 anti-turbulence screens able to individually be lifted out of the settling chamber, thus conveniently allowing variation of free-stream turbulence. Different combinations of turbulence screens were employed to control the free-stream turbulence level. The turbulence intensities associated to each screen configuration were measured with a single hot wire, located in the free-stream upstream of the model at null incidence ($\alpha = 0$), applying a bandpass filter between 2Hz and 5kHz. Hot wire measurements were conducted at a sampling rate of 50 kHz for a duration of 10 s, for a total signal length of 500,000 points per free-stream velocity.

Figure 3 shows the spectral characteristics of the flow in the free-stream for U_∞=40 m/s and U_∞=60 m/s. Figure 4 shows the measured free-stream turbulence intensities with varying free-stream velocity for the three turbulence screen configurations studied. It is evident that the majority of fluctuating energy is associated to lower frequencies, specifically very low frequency "breathing" component and pronounced peak around 80Hz at 40m/s and 105Hz for 60m/s, related to the rotation speed of the tunnel fan. In addition, the effect of the active anti0turbulence screens appears highly non-linear, with only 2 screens already being able to significantly reduce the free-stream turbulence levels. Using all 9 anti-turbulence screens further reduces freestream fluctuations to excellent levels.

Due to the behavior of the tunnel, the decision was made to investigate only modest turbulence levels, and not pursue an artificial increase using turbulence grids. One additional complexity in that scenario is the known effect of high turbulence levels towards triggering travelling crossflow modes [9] [14] [5] whose characteristics are difficult to quantify via thermography. Rather, the present study focuses on the stationary crossflow instability, which prevails in the low-turbulence flight environment.

C. Surface Roughness variations

Two-dimensional sheets of varying roughness were also applied to the model, with root-mean-square (RMS) roughnesses R_q of 1.5 µm, 2.5 µm, and 10 µm, to quantify the effect of distributed surface roughness on the transient growth of stationary crossflow modes. The base roughness of the polished wing model is of 0.20 µm. Dust contamination was kept at a minimum by performing all measurements with the wind tunnel on. Note that, for the reasons explained in section II, turbulence and roughness are uncoupled, in the sense that turbulence is varied only in the clean (R_q = 0.20 µm) roughness case and roughness is varied only with all turbulence screens enabled (Tu/U_∞ = 0.020%).

The RMS roughness R_q was measured using a Mitutoyo SJ-310 mechanical surface profilometer. Long wavelength components in the primary profile of the sheet are removed by applying a high pass filter. The evaluation length and cutoff length were set to 4.0 mm and 0.8 mm respectively. The scans were conducted with a vertical resolution of 5.0 µm/cm and a horizontal resolution of 200.0 µm/cm. Several locations near the leading edge of the model were randomly sampled using the profilometer and averaged in order to arrive to a statistically significant evaluation of surface roughness, summarised in Table 1.

IV. Results and Discussion

A. Laminar-Turbulent Transition

Figure 5 shows the crossflow transition front for three flow cases at different free-stream turbulence intensity. The turbulence intensity increases from (a) to (c) and can be seen moving transition upstream. Figure 7 shows the mean transition location for all flow cases studied. Rising levels of turbulence are found to destabilize the boundary layer and displace the transition front upstream, which is in accordance with previous studies [9] [5]. Consistent and quantifiable losses of laminarity are observed with rising turbulence within the range explored in this campaign. Increasing the turbulence intensity to 0.067% induces losses of laminarity of up to $0.08c_X$, and increasing it to 0.036% leads to losses up to $0.05c_X$ of laminar flow. It is also interesting to note that the largest loss of laminarity is consistently observed when moving from the first to the second screen configuration, although this generates a significantly smaller rise in free-stream turbulence than moving from the second to the third screen configuration; the shift of the transition location is non-linear with respect to rising free-stream turbulence.

Moreover, all turbulence cases explored reveal a similar relationship between mean transition location and angle of attack. At low angles of attack, as transition starts to become crossflow-dominated, large losses of laminarity are observed. The traditional sawtooth pattern first appears and then gradually expands chordwise; in this region (up to $\alpha \approx 2.5$ for Re = $3.39{\cdot}10^6$ and up to $\alpha \approx 1.25$ for Re = $5.07{\cdot}10^6$), mean transition varies steeply with angle of attack. When the sawtooth pattern has regularized and turbulent wedges extend along the entire chord length, the transition location is found to be less sensitive to changes

U_∞ [m/s]	Tu/U_∞ [%]	R_q [µm]	α range [°]	$\Delta\alpha$ [°]	Re_{av} [$\cdot 10^6$]
40	0.020; 0.027; 0.036	0.20	[1.0, 5.0]	0.25	3.39
40	0.020	0.20; 1.50; 2.50; 10.0	[0.0, 3.5]	0.50	3.39
60	0.024; 0.029; 0.067	0.20	[0.0, 3.5]	0.25	5.07

Table 1. Overview of the flow cases analyzed in this study. Re_{av} is the average Reynolds number and $\Delta\alpha$ is the step with which the angle of attack α was varied.

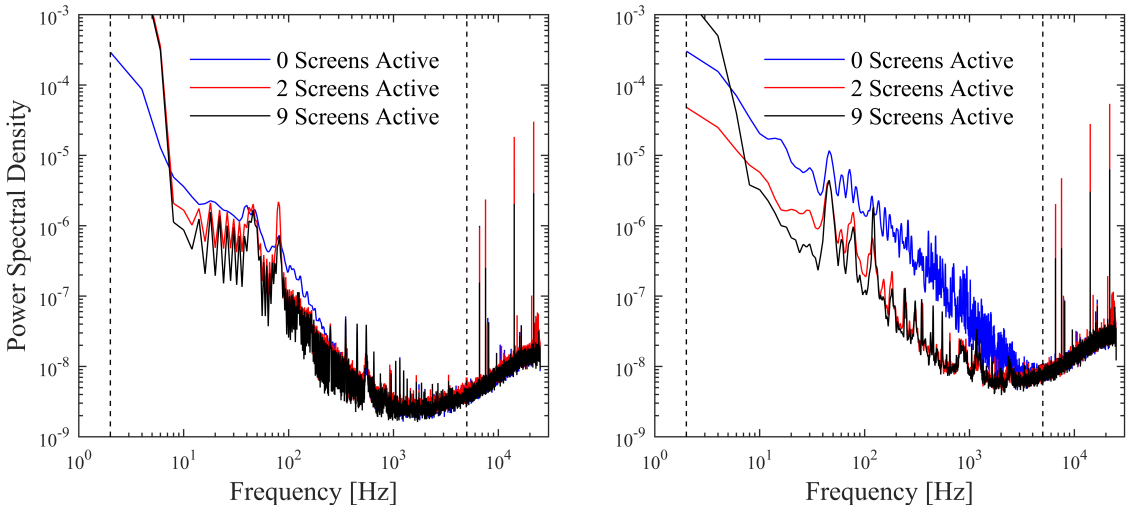

(a) U_∞ = 40 m/s **(b)** U_∞ = 60 m/s

Figure 3. Power spectral density of the fluctuations in free-stream velocity for different combinations of turbulence screens and free-stream velocities. Unfiltered data. The dotted vertical lines represent the bandpass filter between 2 Hz and 5 kHz applied to calculate the free-stream turbulence intensity (Figure 4.)

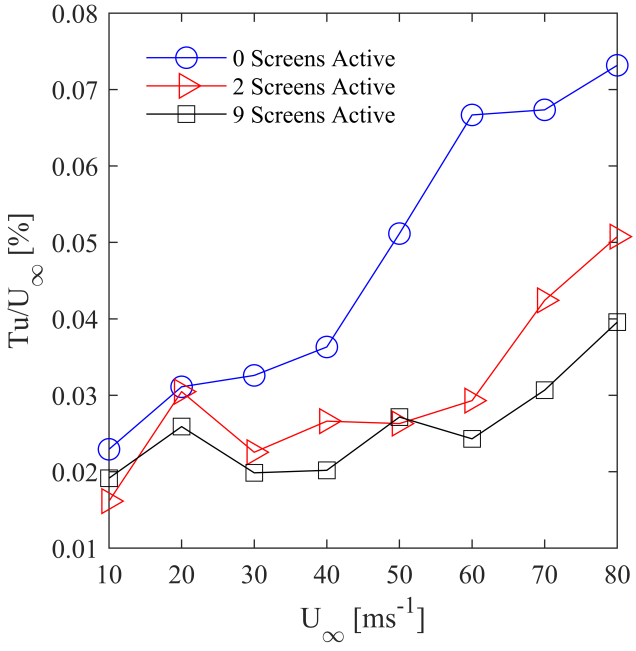

Figure 4. Turbulence intensity measured in the LTT wind tunnel at Delft University of Technology for different free-stream velocities and combinations of turbulence screens. Bandpass filtered data between 2 Hz and 5 kHz.

in angle of attack. The fact that the curves in Figure 7 can be seen changing slope at a similar angle of attack regardless of turbulence intensity indicates that this mechanism is consistent for all turbulence intensities explored.

Increasing the Reynolds number was found to shift crossflow transition upstream significantly; for instance, an average loss of laminarity of $\approx 0.2c_X$ was observed while increasing Reynolds number from $3.39{\cdot}10^6$ to $5.07{\cdot}10^6$ at an angle of attack of 2°. Increasing Reynolds number was also found to accelerate the development of crossflow disturbances; turbulent wedges appeared earlier and regularized over a narrower range of angles of attack, suggesting that higher Reynolds numbers provide the conditions for greater boundary layer receptivity to crossflow instability and faster amplification of the instability. This is consistent with the thinning of the laminar boundary layer near the leading edge at higher Reynolds numbers.

Downs and White [9] observe a notable decrease in transition front width with higher turbulence intensities (up to ≈ 0.19 %). This effect is to be attributed to the fact that higher turbulence intensities promote the amplification of travelling crossflow modes, which propagate perpendicularly to the local streamlines [7] and generate a flatter and less jagged transition pattern than their stationary coun-

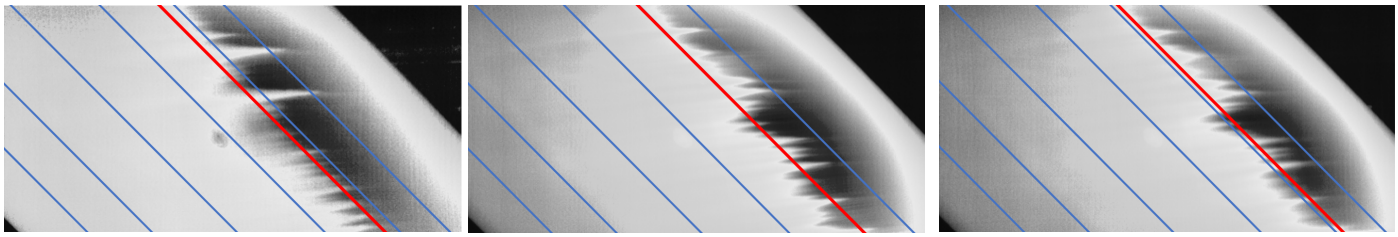

(a) $Tu/U_\infty = 0.020\%$ **(b)** $Tu/U_\infty = 0.027\%$ **(c)** $Tu/U_\infty = 0.036\%$

Figure 5. Thermographic images of the wing at an angle of attack of 4.25°, and Re = 3.39 ·10^6 at different levels of free-stream turbulence intensity. The surface roughness is kept constant at R_q = 0.20 μ m. The red line marks the mean transition location. The blue lines mark the following chord stations [X/c_X] from right to left: 0.10, 0.22, 0.33, 0.45, 0.61, 0.74. Flow comes from right to left. Dark regions denote higher temperature.

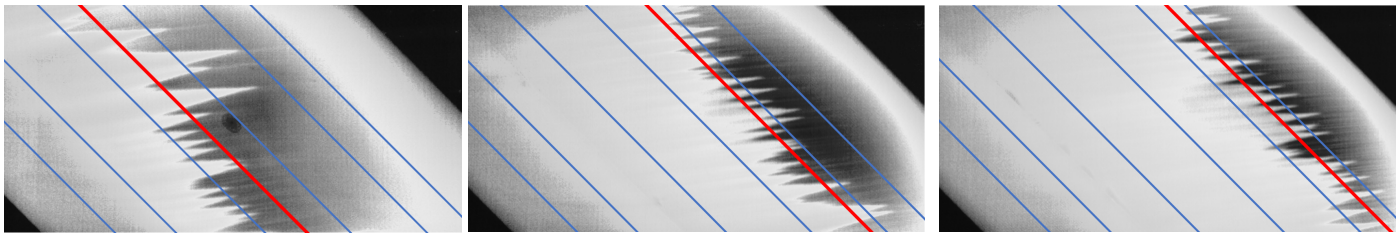

(a) $R_q = 0.20$ μm **(b)** $R_q = 1.5$ μm **(c)** $R_q = 10.0$ μm

Figure 6. Thermographic images of the wing at an angle of attack of 2.00°, and Re = 3.39 ·10^6 at different levels of RMS roughness R_q. The free-stream turbulence intensity is kept constant at Tu/U_∞ = 0.020%. The red line marks the mean transition location. The blue lines mark the following chord stations [X/c_X] from right to left: 0.10, 0.22, 0.33, 0.45, 0.61, 0.74. Flow comes from right to left. Dark regions denote higher temperature.

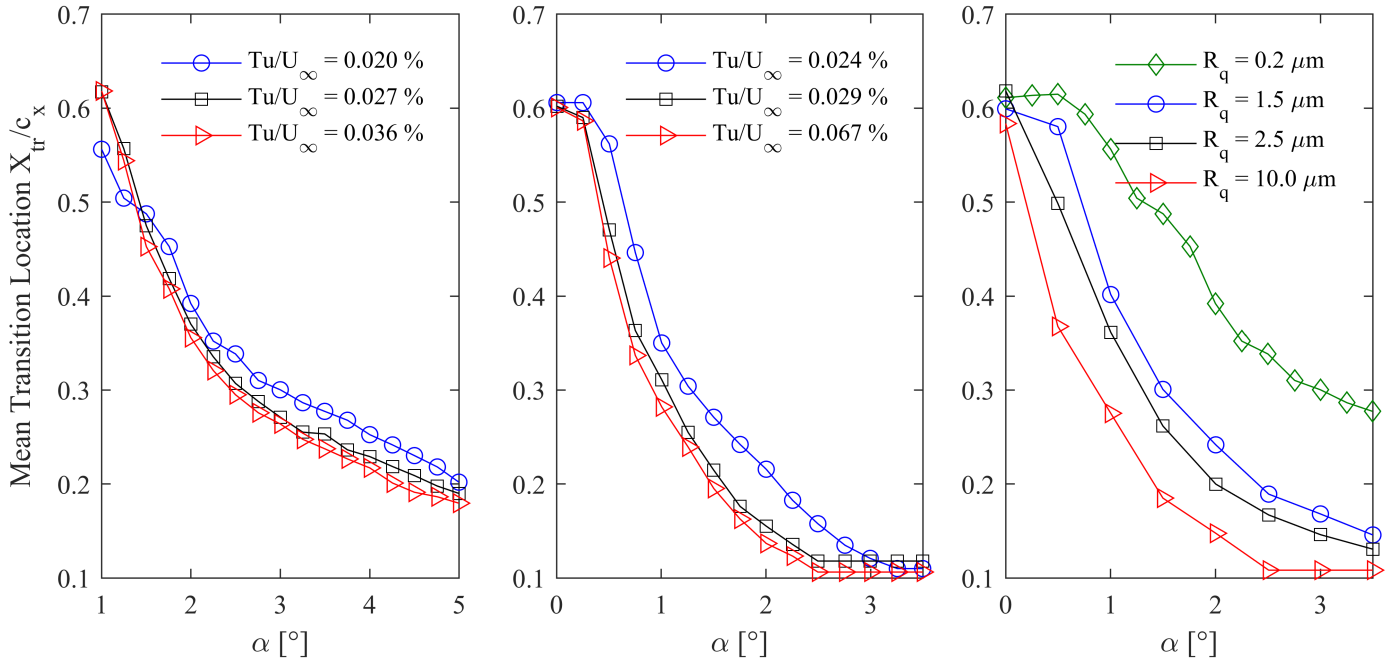

(a) Re = 3.39·10^6, R_q = 0.20 μm. **(b)** Re = 5.07·10^6, R_q = 0.20 μm. **(c)** Re = 3.39·10^6, Tu/U_∞ = 0.020%.

Figure 7. Mean transition location plotted against angle of attack for different values of free-stream turbulence intensity ((a) and (b)) and surface roughness (c) at two Reynolds numbers.

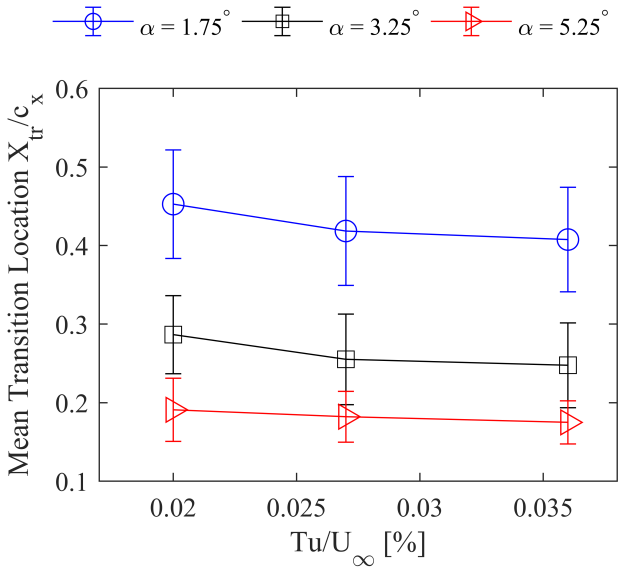

Figure 8. Mean transition location against free-stream turbulence intensity at free-stream velocity of 40 [m/s], Re = 3.39·10^6 and three angles of attack. The error bars represent the jaggedness j of the transition front, a normalized measure of its width (see Equation 1).

terparts. In this study, we monitor the variation in the width of the turbulent wedges of the front by measuring the 'jaggedness' (j) of the sawtooth pattern, which is defined as follows:

$$\mathrm{j} = \left| M\left(X^{\mathrm{p}}_{\mathrm{tr}} + \sigma_{tr}\right) - \left(\frac{X_{\mathrm{tr}}}{c_X}\right) \right| \tag{1}$$

Where $X^{\mathrm{p}}_{\mathrm{tr}}$ is the mean transition location in pixel, σ_{tr} is the standard deviation of points on the transition front about their mean, and M is the spatial coordinate mapping $M : X^{\mathrm{p}} \rightarrow \left(\frac{X}{c_X}\right)$ obtained from calibration. As shown in Figure 8, no notable or consistent decrease in the front's jaggedness with rising turbulence intensity was observed. This suggests that the traveling instability was not amplified enough to noticeably erode the front for the turbulence intensities explored. This is consistent with the aim of the campaign to focus solely on the stationary instability, and reproduce experimental conditions in which the stationary instability dominates transition.

Surface roughness is found to further destabilize the boundary layer and move crossflow transition upstream. Large losses of laminarity are incurred in the presence of the distributed roughness sheets: at α = 1.00°, these losses are up to $\approx 0.30c_X$ at 10 µm, $\approx 0.23c_X$ at 2.5 µm and $\approx 0.20c_X$ at 1.5 µm. Figure 6 shows the crossflow transition front for three flows that are identical besides the roughness level, which increases from (a) to (c) and moves transition upstream.

At higher roughness levels, crossflow transition behavior is evident at lower angles of attack. At 10 µm, turbulent wedges are already present at neutral incidence, and at an angle of attack of 0.5°a sawtooth pattern covers the entire chord. In the other two roughness cases, no evidence of crossflow transition is present at the same angles of attack. Surface roughness also does not appear to have a consistent effect on transition front width, other than for the lowest angles of attack, when turbulent wedges are only present with higher roughness. This suggests that distributed surface roughness provides conditions that promote the amplification of stationary disturbances, without largely amplifying their traveling counterparts.

B. Linear Stability Theory

Linear Stability Theory (LST) has proven to be a powerful tool in predicting the onset, spatial growth and frequency of primary crossflow modes (see [14] [1] [11] [12] [10]). In this study, LST was used to complement experimental transition data in order to draw conclusions regarding the growth of specific crossflow instability modes.

To this end, the spatial formulation of the linear stability problem with a two-dimensional disturbance was solved for the boundary layer over the model pressure side. Equation 2 shows that in the linear stability framework, disturbances are expressed as spatio-temporally evolving waves with a two-dimensional wavenumber vector. Complex parameters α ($\alpha_r + i\alpha_i$) and β ($\beta_r + i\beta_i$) are the streamwise and spanwise components of the wavenumber vector respectively, ω is the angular frequency and $q(y)$ is the perturbation eigenfunction.

$$q'(x, y, z, t) = \bar{q}(y)e^{i(\alpha x + \beta z - \omega t)} \tag{2}$$

The resulting quartic eigenvalue problem was solved via the Chebyshev collocation method, using 100 polynomials and exploiting the companion matrix technique [6] to handle non-linearity to the eigenvalue. The boundary layer associated to the measured pressure distribution, instead, was computed by means of a solver based on the steady, incompressible boundary layer equations. A Crank-Nicholoson implicit discretization was used and validation was performed via comparison with Falkner-Skan-Cooke solutions.

Spanwise flow invariance entails the assumption of null growth rates in the z-direction ($\beta_i = 0$), and greatly simplifies the computation of a given mode's amplification N-factor. Under this assumption, the latter can be evaluated at any chordwise station by integrating the exponential chordwise growth rate of the perturbations ($-\alpha_i$)

starting from the first unstable station x_0.

$$N(x, \lambda_z, \omega) = \int_{x_0(\lambda_z,\omega)}^{x} -\alpha_i(\zeta, \lambda_z, \omega) d\zeta \qquad (3)$$

Due to the very low base turbulence intensity of the facility and the low range of turbulence intensities explored in this campaign, it was deemed appropriate to track only stationary (ω = 0) crossflow modes. It is likely, however, that travelling modes were also amplified, albeit to a lesser extent. The most unstable mode at the transition location and the associated critical N-factor was identified by considering the envelope of all the unstable modes with constant z-wavelength λ_z.

$$N^{env}(x) = \max|_{\lambda_z} (N(x, \lambda_z)) \qquad (4)$$

$$N^{SCF} = N^{env}(x = X_{tr}) \qquad (5)$$

The mean transition location X_{tr} was computed from thermographic scans of the pressure side of the model as discussed in section III. Figure 9 shows the streamwise evolution of several instability modes for a single flow case, and illustrates the extraction of the critical transition N-factor N^{SCF}.

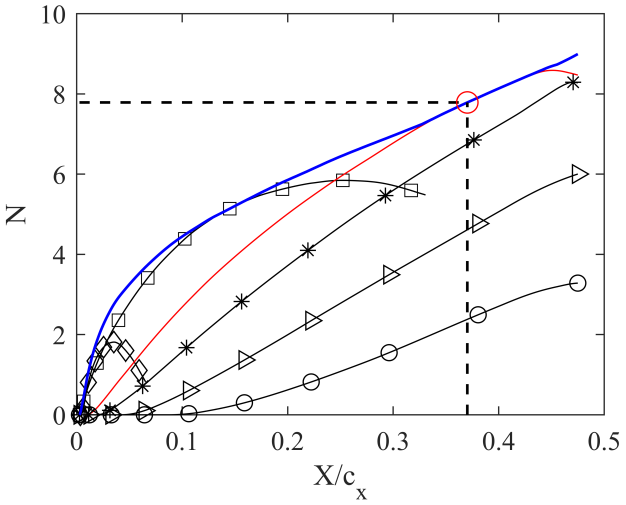

Figure 9. Streamwise evolution of several crossflow instability modes as retrieved via LST analysis for a single flow case. In this case $\alpha = 2°$, U_∞ = 40 m/s and Re = 3.39·10^6. The red curve represents the most amplified mode at the transition location (λ_z = 6 mm), and the blue line represents the N-factor envelope N^{env}. The dotted line intercepts the x-axis at the transition location (X_{tr}/c_X) determined experimentally, and intercepts the y-axis at the transition N-factor of the critical stationary crossflow instability (N^{SCF}). The solid black lines represent the following crossflow modes: ◯: λ_z =18 mm, ▷ : λ_z =12 mm, ∗: λ_z =8 mm, □: λ_z =4 mm, ◇: λ_z =2 mm.

,

Figure 10 (a) and (b) show the transition N-factor of the critical stationary crossflow instability (N^{SCF}) as a function of turbulence level at two different Reynolds numbers and several low angles of attack. The transition N-factors show a clear dependence on turbulence level for the angles of attack and Reynolds numbers considered; higher turbulence intensities allow the stationary instability to grow less in amplitude as transition moves upstream. It is interesting to note that the critical N-factors appear to cluster over specific incidence angles. For instance, in Figure 10 (a) there is a clear distinction between the range $1.75 \leq \alpha \leq 2.50$ and $2.75 \leq \alpha \leq 3.50$; this may be due to boundary layer receptivity to the instability being particularly sensitive to specific changes in angle of attack and reacting non-linearly to these changes.

Figure 10 (c) shows N^{SCF} as a function of surface roughness for several low angles of attack at Re = 3.39 ·10^6. For all angles of attack considered, the transition N-factor of the stationary instability scales approximately with the log of the roughness level; this is consistent with a linear receptivity mechanism and agrees well with the findings of Radetsky et al. [13] and Crouch and Ng [5][4].

V. Conclusion

This study considered the evolution of crossflow transition of the boundary layer over a 45°swept wing under varying Reynolds number, free-stream turbulence, angle of attack and surface roughness. The transition front was first analyzed by means of thermography in order to quantify the mean transition location and jaggedness (standardized width) of the crossflow sawtooth pattern. These measurements were complemented with LST to determine the transition N-factor of the dominant stationary crossflow instability. Results show clear causality between free-stream turbulence, surface roughness and the critical N-factors. N-factor sensitivity to free-stream turbulence varies significantly with angle of attack, whereas the N-factors scale linearly with the log of the surface roughness level regardless of the angle of attack.

References

[1] D. Arnal, G. Gasparian, and H. Salinas. “Recent advances in theoretical methods for laminar-turbulent transition prediction”. In: *AIAA Paper 1998-0223* (1998).

[2] H. Bippes. “Basic experiments on transition in three-dimensional boundary layers dominated by crossflow instability.” In: *Prog. Aerospace Sci.* 35.4 (1999), pp. 363–412.

[3] J.D. Crouch, V.S. Kosorygin, and L.L. Ng. “Modeling the effects of steps on boundary-layer transition”. In: *Sixth IUTAM Symposium on Laminar-Turbulent Transition* (2006), pp. 37–44.

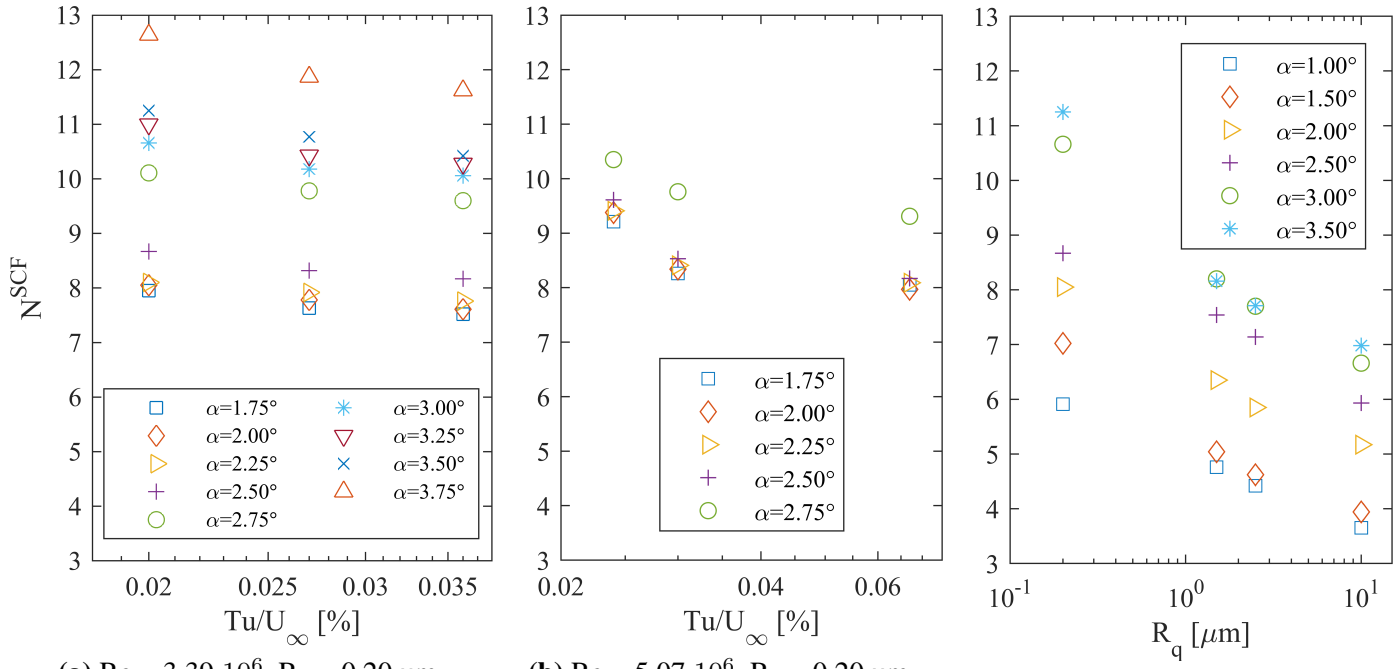

(a) Re = $3.39 \cdot 10^6$, R_q = 0.20 µm. **(b)** Re = $5.07 \cdot 10^6$, R_q = 0.20 µm. **(c)** Re = $3.39 \cdot 10^6$, Tu/U_∞ = 0.020%.

Figure 10. Stationary crossflow transition N-factors as retrieved via LST, plotted against free-stream turbulence ((a) and (b)) and surface roughness (c) at several angles of attack and two Reynolds numbers.

[4] J.D. Crouch and L.L. Ng. "Variable N-Factor Method for Transition Prediction in Three-Dimensional Boundary Layers". In: *AIAA J.* 38.2 (2000), pp. 211–216.

[5] J.D. Crouch et al. "Influence of surface roughness and free-stream turbulence on crossflow-instability transition". In: *Procedia IUTAM Symposium on Laminar Turbulent Transition* 14 (2015), pp. 295–302.

[6] G. Danabasoglu and S. Biringen. "A Chebyshev matrix method for the spatial modes of the Orr-Somerfeld equation". In: *International Journal for Numerical Methods in Fluids* 11.7 (1990), pp. 1033–1037.

[7] H. Deyhle, G. Hohler, and H. Bippes. "Experimental investigation of instability wave propagation in a three-dimensional boundary-layer flow". In: *AIAA J.* 31.4 (1993), pp. 637–645.

[8] H. Deyle and H. Bippes. "Disturbance growth in an unstable three-dimensional boundary layer and its dependence on environmental conditions". In: *J. Fluid Mech.* 316 (1996), pp. 73–113.

[9] Robert S. Downs and Edward B. White. "Free-stream turbulence and the development of cross-flow disturbances". In: *J. Fluid Mech.* 735 (2013), pp. 347–380.

[10] T.S. Haynes and H. L. Reed. "Simulation of swept-wing vortices using nonlinear parabolized stability equations". In: *J. Fluid Mech.* 405 (2000), pp. 325–349.

[11] M. Hogberg and D. Henningson. "Secondary instability of cross-flow vortices in Falkner–Skan–Cooke boundary layers". In: *J. Fluid Mech.* 368 (1998), pp. 339–357.

[12] M.R. Malik, F. Li, and C.-L. Chang. "Crossflow disturbances in three-dimensional boundary layers: nonlinear development, wave interaction and secondary instability". In: *J. Fluid Mech.* 268 (1998), pp. 1–36.

[13] R.H. Radeztsky et al. "Effect of micron-sized roughness on transition in swept-wing flows". In: *AIAA Paper 93-0076* (1993).

[14] M. S. Reibert et al. "Experiments in nonlinear saturation of stationary crossflow vortices in a swept-wing boundary layer". In: *American Institute of Aeronautics and Astronautics* AIAA Paper 96-0184 (1996).

[15] W. S. Saric, H. L. Reed, and E. B. White. "Stability and transition of three-dimensional boundary layers". In: *Annu. Rev. Fluid Mech.* 35 (2003), pp. 413–440.

[16] W.S. Saric, A.L. Carpenter, and H.L. Reed. "Passive control of transition in three-dimensional boundary layers, with emphasis on discrete roughness elements." In: *Philos Trans A Math Phys Eng Sci.* 369.1940 (2011), pp. 1352–1364.

[17] J. Serpieri and M. Kotsonis. "Flow visualization of swept wing boundary layer transition". In: *10th Pacific Symposium on Flow Visualization and Image Processing* (2015).

[18] J. Serpieri and M. Kotsonis. "Three-dimensional organisation of primary and secondary crossflow instability". In: *J. Fluid Mech.* 799 (2016), pp. 200–245.

[19] J. Serpieri, S.Y. Venkata, and M. Kotsonis. "Conditioning of cross-flow instability modes using dielectric barrier discharge plasma actuators". In: *J. Fluid Mech.* (2017), pp. 14–205.

[20] Y.X. Wang and M. Gaster. "Effect of surface steps on boundary layer transition". In: *Experiments in Fluids* 39 (2005), pp. 679–686.

[21] P. Wassermann and M. Kloker. "Mechanisms and passive control of crossflow-vortex-induced transition in a three-dimensional boundary layer". In: *J. Fluid Mech.* 456 (2002), pp. 49–84.

[22] S. Yadala et al. "Experimental control of swept-wing transition through base-flow modification by plasma actuators". In: *J. Fluid Mech* 844.R2 (2018).